Article

Smartphone administered pulsed radio frequency energy therapy for expedited cutaneous wound healing

Check for updates

Mengxia Yu [1,2], Hongjia Yang [2,3], Haoteng Ye [2], Shuhuang Lin [4], Yujie Lu [2], Haoqiang Deng [2], Lulu Xu [5], Yongxin Guo [6] ✉, John S. Ho [1,7,8] ✉ & Terry Tao Ye [2,9] ✉

Pulsed radio frequency energy (PRFE) therapy is a non-invasive, electromagnetic field-based treatment modality successfully used in clinical applications. However, conventional PRFE devices are often bulky, expensive, and require extended treatment durations, limiting patient adherence and efficacy. Here, we present a lightweight, cost-effective wearable PRFE system consisting of a flexible electronic bandage and a smartphone. The bandage, mainly composed of an NFC Frequency Doubler (NFD) and a Radiofrequency Energy Radiator (RER), is powered and administered by the smartphone to generate 27.12 MHz radio wave pulses, for simplified, smartphone-enabled PRFE therapy. Its ultra-flexible, battery-free design supports personalized wound care at a low-cost (<US$1). Both electromagnetic field simulation and measurement demonstrated that the proposed PRFE bandage achieves the field strength of clinical-grade PRFE equipment. In rat full-thickness wound models, PRFE therapy improved wound closure rates by ~20%, with enhanced re-epithelialization and angiogenesis compared to controls.

Cutaneous wounds are among the most common injuries experienced in daily life, and effective and affordable therapy for cutaneous wound healing is much desired[1–3]. Throughout human history, bandages have been the most convenient method for cutaneous wound treatment and remain a popular choice for general households in addressing minor injuries. While conventional bandages are fundamental in managing bacterial infections, aiding wound closure and tissue repair, their effectiveness is limited in challenging environments such as wilderness or battlefield conditions[4–7] where frequent changes are impractical. Electrotherapy, including Electrical Stimulation (ES), Near-Infrared (NIR) radiation, and Pulsed Radio Frequency Energy (PRFE) treatments[8–14], has become a complementary and effective therapy for cutaneous wounds[8,12–21]. However, some reported electrotherapy devices (Supplementary Table 1) are often cumbersome and reliant on battery-driven metal components[22–27], posing risks such as discomfort and potential metal-induced infections. Moreover, these devices typically require direct contact with metal electrodes[10,14,28], involve lengthy treatment[14,24,26] and extensive circuitry, and lack flexibility, which can significantly lower patient compliance and adaptability to various wound types.

Among these electrotherapeutic methods, PRFE therapy has been regarded as an effective treatment to accelerate wound healing[29,30]. Typical PRFE treatment in clinical uses an electromagnetic carrier wave at the high frequency (HF) band (13 MHz–27.12 MHz), with pulse duration from a few tens of μsec to a few tens of msec intervals (pulse frequency 2 Hz–1 kHz)[12] and applied directly at the targeted tissues, as illustrated in Fig. 1a. PRFE is thought to stimulate cellular proliferation by enhancing the endogenous electric field in tissues[23,31,32]. This enhancement facilitates the opening of transmembrane ion channels, increases cytoplasmic free ions (like Ca^{2+}), and initiates a cascade of secondary effects[23,25,33–39] (Fig. 1b). PRFE is commonly utilized in postoperative recovery, plays a role in promoting wound healing for chronic ulcers, and addresses various wound conditions[21,40–44].

Since its invention in 1935[45], PRFE has been successfully proven to facilitate heat dissipation between pulses and minimize tissue thermal effect and become more prevalent than continuous RF therapy[46–48]. Besides, PRFE

[1]Department of Electrical and Computer Engineering, National University of Singapore, Singapore, Singapore. [2]Department of Electrical and Electronic Engineering, Southern University of Science and Technology, Shenzhen, China. [3]School of Biomedical Engineering, Tsinghua University, Beijing, China. [4]School of Medicine, Southern University of Science and Technology, Shenzhen, China. [5]The Wolfson School of Mechanical, Electrical and Manufacturing Engineering, Loughborough University, Loughborough, UK. [6]Department of Electrical Engineering, City University of Hong Kong, Hong Kong, China. [7]The N.1 Institute for Health, National University of Singapore, Singapore, Singapore. [8]Institute for Health Innovation and Technology, National University of Singapore, Singapore, Singapore. [9]Institute of Nanoscience and Applications, Southern University of Science and Technology, Shenzhen, China. ✉e-mail: yongxin.guo@nus.edu.sg; johnho@nus.edu.sg; yet@sustech.edu.cn
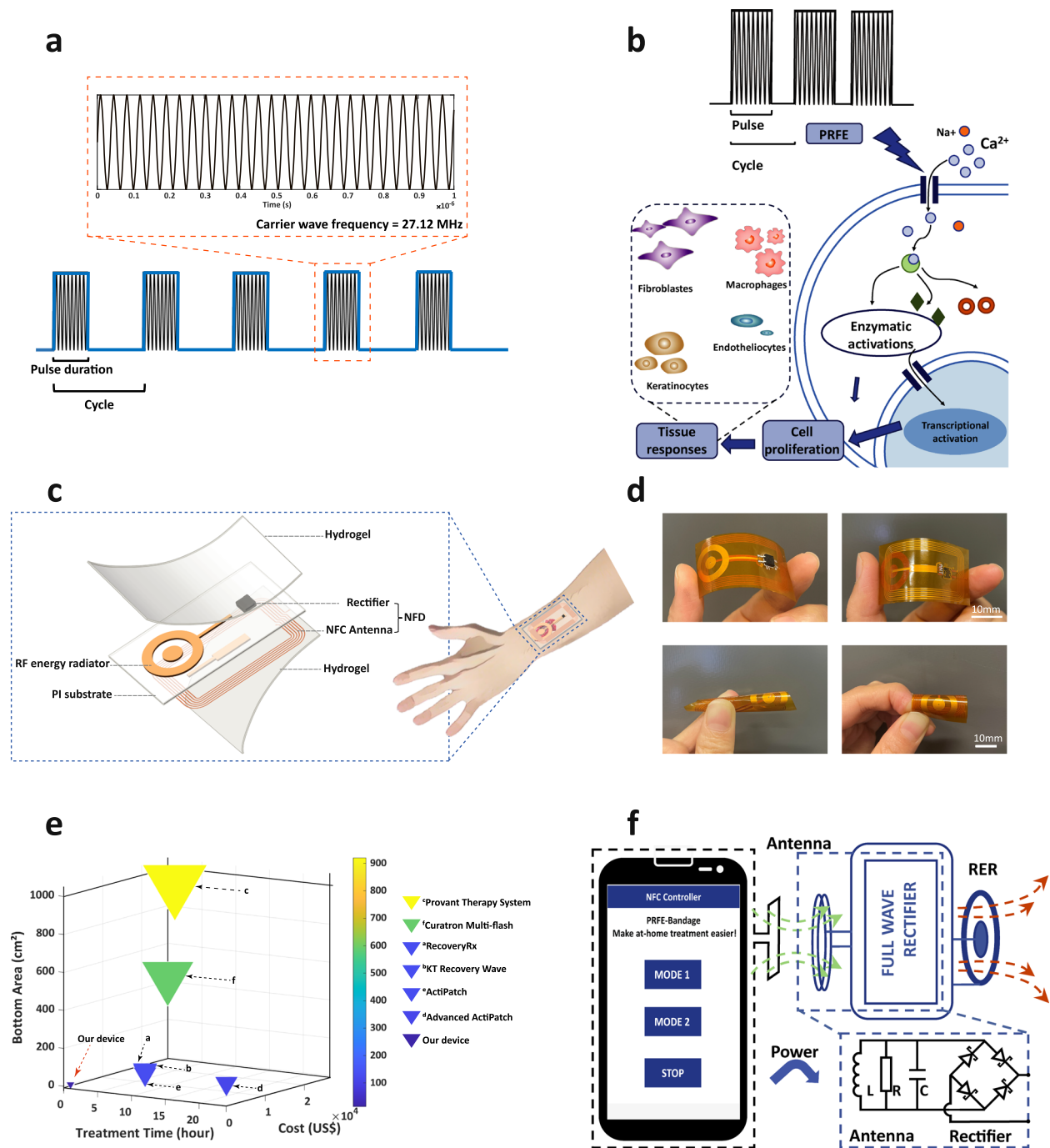
Fig. 1 | System structure of the PRFE-Bandage. a Illustration of the pulsed RF shortwave generated by PRFE devices. **b** Schematic diagram showing biophysical effect for promoting wound healing triggered by the PRFE therapy. **c** Exploded view showcasing the double-layer structure of the PRFE-Bandage (left), comprising NFD (an energy harvesting antenna connected with a full-bridge rectifier), and RER (radiation electrode ring), integrated on a flexible PI substrate and encapsulated with hydrogels, and schematic illustration of the proposed PRFE-Bandage mounted on a forearm wound (right). **d** Photographic depiction of various angles of the PRFE-Bandage (front side - upper left, back side - upper right; curled along long side - lower left, and by short side - lower right), highlighting its high flexibility. **e** Comparison of reported clinical PRFE treatment devices with our PRFE Bandage in daily treatment time, cost, and bottom area. (Colormap and triangles size map different levels of bottom areas). **f** The PRFE-Bandage is paired with a smartphone through the NFC function during treatment, and the APP is installed on the smartphone for treatment administration.

devices precisely deliver treatment energy to targeted tissues, making it an optimal choice for localized and non-invasive treatments[49,50]. However, existing PRFE devices typically require stable power supplies or high-capacity batteries and feature sophisticated circuitry with solid-state components[20,47,51,52]. Due to their bulky structures (for example, the Provant Therapy System measures 35.1 × 26.2 × 15.2 cm and weighs 4535.9 g), high costs (exceeding US$20,000), and complex operating procedures, these devices are predominantly limited to clinical settings. There is a growing demand for a flexible, low-cost, easily accessible PRFE treatment method suitable for daily at-home care and for individuals in conditions not accessible to clinical treatments[12,53].

In this paper, we propose a convenient apparatus for PRFE treatment, a cost-effective, ultra-flexible, and personalized bandage, termed as the "PRFE-Bandage", that can be administered conveniently from a
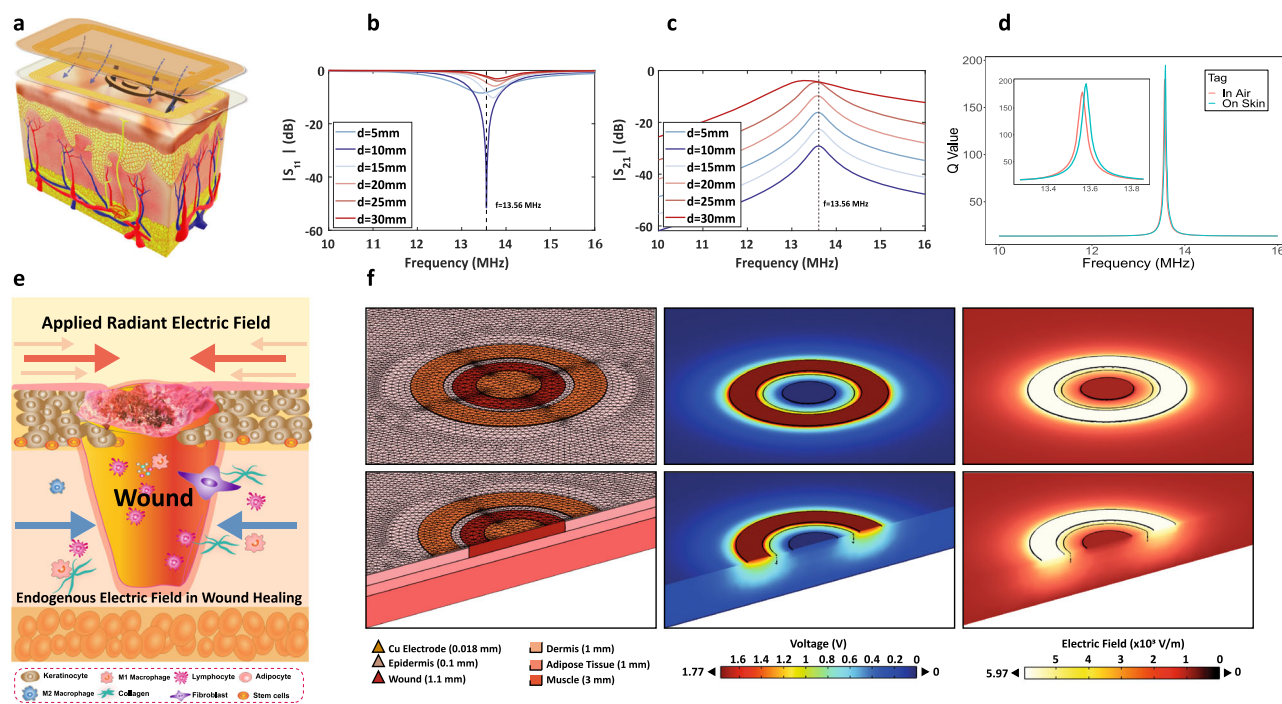
Fig. 2 | Modeling and simulation of the electromagnetic properties of the PRFE-Bandage during cutaneous wound treatment. a 3D illustration of the PRFE-Bandage on skin tissues. **b, c** |S11| and |S21| parameters under different operation distances from 5 mm to 30 mm between the PRFE-Bandage and the smartphone. **d** Q-factor of the PRFE-Bandage resonating antenna. **e** Schematics illustrating enhance the wound-induced endogenous electric field by external electric field to facilitate wound healing. **f** Computational results for the distribution of the mesh view (left), the voltage (middle), and the electric field (right) in vivo wound conditions. The wound model contains layers of epidermis, dermis, adipose, and muscle, and the RER structure contains copper internal and external electrodes.

smartphone. The PRFE-Bandage harvests energy from the NFC function of a smartphone and can generate pulse waveforms similar in magnitude and directivity to those produced by clinical PRFE treatment devices[12,21]. The proposed PRFE-Bandage consists of a frequency doubler and an RF energy concentrator, constructed solely with passive components on highly flexible and water-resilient substrates, ensuring robustness under stress and functionality in moisture and liquid environments. The PRFE-Bandage can operate without batteries, drawing wireless power from the smartphone and administering therapeutic doses from the application programs (APP) on the smartphone. The PRFE-Bandage can also be tailored to accommodate the shapes of the wound formations. We further verify the effectiveness of the PRFE-Bandage through animal wound modeling on rats, and demonstrate that PRFE-Bandage accelerates wound healing and microvascular formation by enhancing the wound closure rate, promoting epithelial cell migration and angiogenesis, and reducing scar tissue.

Results

The structure of the PRFE-Bandage

The PRFE-Bandage features ultra-thin, battery-free, flexible circuitry on a skin-friendly substrate. The circuit only uses passive components, i.e., an NFC Frequency Doubler (NFD), and a Radiofrequency Energy Radiator (RER), as depicted in Fig. 1c and Supplementary Fig. 1 (dimensional design details). The NFD structure consists of an NFC antenna, which is a single-layer coil (copper-clad laminated on polyimide (PI) substrate) resonating at the NFC frequency of 13.56 MHz. The coil is connected to a diode full-bridge rectifier, which doubles the input NFC signals into the rectified DC signals oscillating at 27.12 MHz. A capacitor that follows blocks the DC components and generates a carrier wave with a frequency of 27.12 MHz. This frequency falls into the Industrial, Scientific, and Medical (ISM) channel, which is also allocated by the U.S. Food and Drug Administration (FDA) for therapeutic devices[12,19,54]. The RER structure consists of an electromagnetic radiator with a pair of ring electrodes, enclosed in a thin encapsulation layer made of PI as a protective barrier to prevent direct contact between the metal electrodes and the wound. The outer ring electrode of RER represents the anode and the central circular inner ring represents the cathode. The cathode on the Side A is interconnected with the electrode (grounded) on the Side B of the FPCB (Supplementary Fig. 2). Over this thin PI layer, a sterile, adhesive hydrogel is applied, ensuring secure attachment to the wound site while minimizing the risk of infection.

The simplicity of the structures enables the PRFE-Bandage to be highly customizable, flexible, and cost-effective. And it also addresses challenges related to wound-device compatibility. By matching the wound sizes to the device's effective treatment area, our design ensures consistent therapy delivery and reliable experimental comparisons. This adaptability highlights the potential for broader clinical applications, as the flexible electrode configuration can accommodate diverse wound shapes and sizes. In this study, we have constructed the PRFE-Bandages with two form-factors, i.e., the one with a circular radiator (PRFE-C) for circular-shaped wounds and the other with rectangular radiator (PRFE-L) for linear incision wounds (the designs illustrated in Supplementary Fig. 3 and Supplementary Fig. 4). The PRFE-Bandage is fabricated on an FPCB, with 26.3 mm of width, 51.3 mm of length, and 130 μm of thickness. It is highly flexible and can be curled along the long edge and the short edge, as shown in Fig. 1d. The PRFE-Bandage is attached with a hydrogel layer, which makes it bio-friendly to wounds, avoiding the metal-induced infection or inflammation caused by directly interfacing with metallic materials, as issues reported from other metallic electrodes designs[14,28,55]. Compared to traditional clinical PRFE treatment devices, our device excels in terms of the smallest size (footprint area = 13.5 cm²), lightest weight (0.34 g), most effective treatment duration (1 h/day), and lowest cost. The PRFE-Bandage can be fabricated at an extremely low cost in mass production, approximately US$1.00 for Bill of Materials (BOM) and manufacturing cost, so it can be disposed of after each use. The comparison of reported clinical PRFE treatment devices with our PRFE Bandage provided in Fig. 1e and Supplementary Table 2 highlights the manufacturing cost of our PRFE-Bandage in relation to the retail cost of commercially available devices.
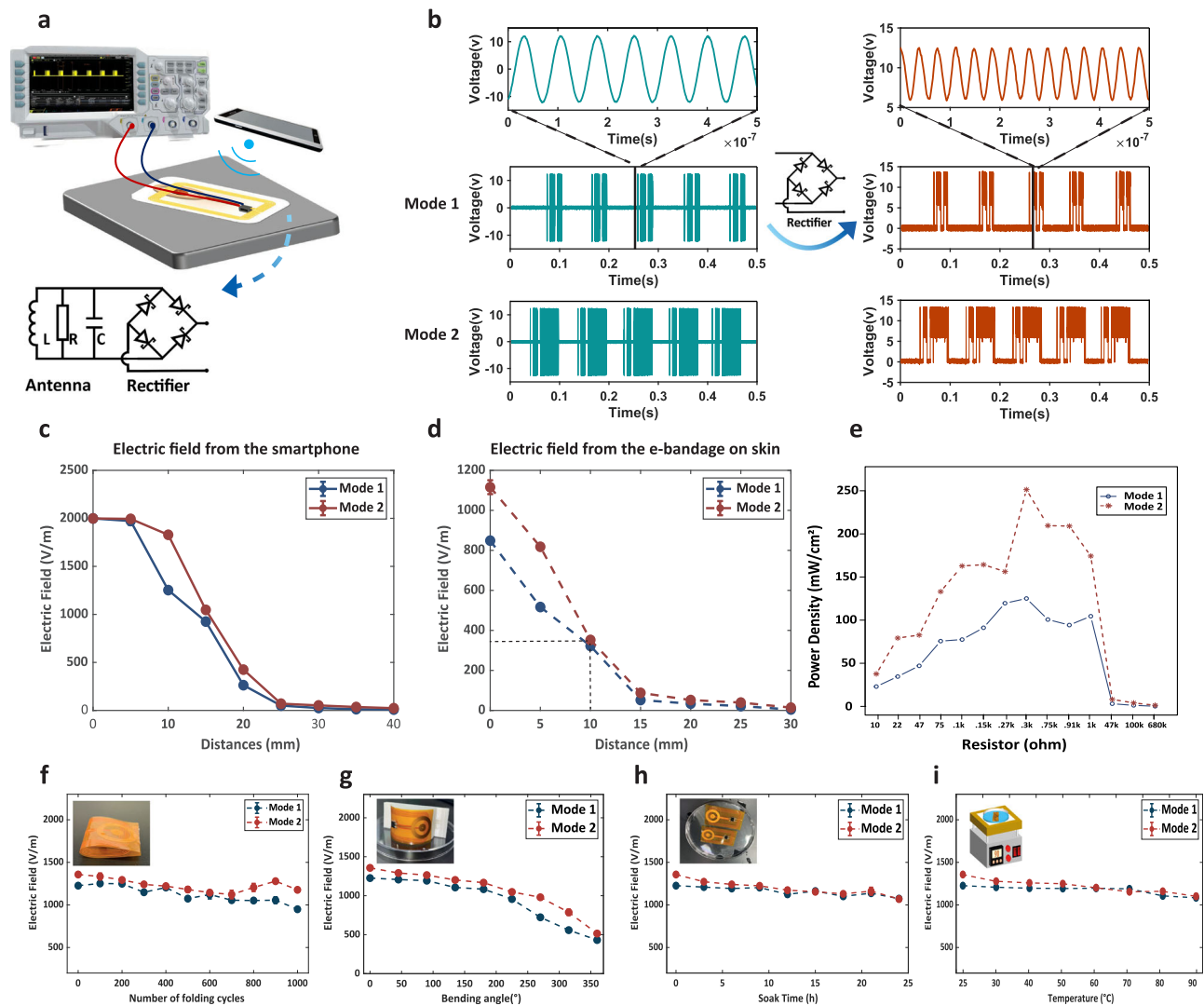
Fig. 3 | Characteristics of two PRFE therapeutic modes. a The experiment setup (an oscilloscope connected with a PRFE-Bandage powered by a smartphone) and an equivalent circuit model of the antenna and the rectifier as the NFD device. **b** Carrier waveforms and pulsed waveforms of two preprogrammed therapeutic modes: NFC carrier frequency at 13.56 MHz and pulsed carrier waves from Mode 1 and Mode 2 (left); Doubled carrier frequency at 27.12 MHz, and pulsed carrier waves from Mode 1 and Mode 2 (right). **c** Electric field strengths at different distances radiated from the NFC-enable smartphone. **d** Electric field strengths on the PRFE-Bandage powered at different distances from the smartphone. **e** Emission power of the radiator electrode ring (RER) of the PRFE-C Bandage under different loads in Mode 1 and Mode 2. **f–i** Stress and durability tests of the PRFE-Bandages ($n = 10$). Electromagnetic field of PRFE-C system under two therapeutic modes as a function of repeated folding cycles (**f**), bending angles (**g**), soaking with 24 h of duration, (**h**) and temperature variation from 25 °C to 90 °C (**i**).

Pulsed radio wave generation and two smartphone-programable therapeutic modes

When the PRFE-Bandage is placed within the NFC reading range of the smartphone, the RER produces steady pulsed signals at the 27.12 MHz carrier wave. By controlling the duty cycle of the NFC signal emission from smartphones, different treatment modes can be programmed. We developed a smartphone app to control the duty cycle of the pulses and preprogrammed two treatment modes to investigate the treatment-dose effect. Figure 1f illustrates the operation and working principle of our PRFE-Bandage system, highlighting two therapeutic modes administered through the smartphone APP's Graphical User Interface (GUI). Both modes employ square amplitude modulation of the carrier wave to generate pulsed envelopes at a frequency of 10 Hz. These modes essentially utilize square amplitude modulation on the carrier wave to produce pulsed envelope waves at a frequency of 10 Hz. Mode 1 is defined by a 30 ms NFC signal 'on' period followed by a 70 ms 'off' period for each pulse cycle, whereas Mode 2 extends the 'on' period to 60 ms with a reduced 'off' period of 40 ms.

RF performance optimization

The complete PRFE apparatus is constructed in electromagnetic simulation software and the PRFE's electromagnetic performance and as well as energy harvesting capability are simulated and optimized, as depicted in Fig. 2a. The construction includes a transmission antenna coil that represents the NFC antenna in the smartphone, a receiving antenna coil that represents the antenna on the PRFE-bandage. A human skin tissue model is also constructed to emulate the electromagnetic ambient conditions when the PRFE-bandage is attached to the skin surface. Various transmission-receiving antenna distances are simulated to find the optimal operating set-up to achieve the maximum power-transfer co-efficiency.

The paired coils were optimized to achieve the minimum $|S11|$ value (−57 dB) at a distance of 10 mm (Fig. 2b). The $|S12|$ parameter reaches its maximum value at a resonant frequency of 13.56 MHz to achieve the optimal energy transmission, as shown in Fig. 2c. The Quality Factor (Q-factor) serves as a crucial parameter for wireless energy transmission and communication, which could be influenced by the skin tissues that behave as an energy-absorbing dielectric layer in high-frequency radio waves. The

Q-factor value at 13.56 MHz of our transmission-reception coil-pair attached to the skin tissues had been optimized to reach similar Q-factor values achieved in the air, as illustrated in Fig. 2d. Experimental measurements using high-frequency (HF)/low-frequency (LF) Tag tester (Supplementary Fig. 5a) confirm that the maximum of Q-factor value remains stable at approximately 30 at 13 MHz (Supplementary Fig. 5b) even when the PRFE-bandage is attached on the skin surface, showing a balance between wireless communication bandwidth and energy harvesting efficiency of the PRFE apparatus (details in "Methods").

Electric field simulation for cutaneous wound around an RER electrode

When a wound is inflicted on the skin tissue, the epithelial layer is disrupted and the epithelial potential is interrupted, triggering the endogenous electric fields (42–100 V/m) at wound sites that facilitate re-epithelialization[8,25]. The PRFE-Bandage enhances the endogenous electric fields through applying an external electric field and initiates a cascade of wound-healing cellular processes, as illustrated in Fig. 2e. We conducted the three-dimensional (3D) finite element analysis (FEA) of the electromagnetic field distribution on the cutaneous wound model under a radiating RER electrode (applied with a rectified signal at 27.12 MHz) (details in "Methods" and Supplementary Table 3). The 3D simulation's mesh view is shown in Fig. 2f (left). Existing literature demonstrates that positioning a cathode at a wound site with an electric field of 12.5–200 V/m could significantly enhance cellular migration into the wound and accelerate epithelial cell migration[8]. The study[25] shows that the electric field rapidly attenuated within the first 2 mm into the skin and slowly decayed to a low value, and localized electric fields ranging could ensure effective treatment at tissue-electrode interfaces. Our FEA simulation reveals a localized maximum electric field strength of approximately 4000 V/m in the epidermis and dermis beneath the RER electrode and ~2500 V/m in the blood region between the inner and outer rings (Fig. 2f, right). By comparison, for example, previously reported serpentine Mo electrodes for skin stimulation produce electric fields around 250 V/m[13]. The higher field strengths in our simulations reflect the focused stimulation capabilities of the RER electrode, which is specifically designed to achieve localized effects near the electrode-tissue interface. The strength of electrical field is tunable from the APPs installed on the smartphone and it is enough to induce the biophysical effect to facilitate the wound healing process[56]. Supplementary Fig. 6 also represents the FEA results for PRFE-L Bandage in cutaneous wound conditions. And the current density distribution of RER is shown in Supplementary Fig. 7. Those simulation results indicate that PRFE-Bandage might effectively accelerate the wound healing process by enhanced electric field.

Electromagnetic characterization under two therapeutic modes

Through the smartphone APP, user could administer the PRFE treatment by programming the pulse parameters such as magnitude, width and intervals, etc. Two different PRFE modes are pre-set to investigate the treatment-dose effect. In Mode 1, NFC signal is turned 'on' time for 30 msec, followed by an 'off' time (interval) of 70 msec per pulse cycle. In Mode 2, the 'on' time is doubled to 60 msec while the 'off' time set at 40 msec, thereby offering longer pulse duration (and therefore more energy) with the same pulse frequency. The carrier waveforms of these two therapeutic modes before and after NFD rectification are illustrated by an oscilloscope (Fig. 3a), while the PRFE-Bandage is powered by the NFC function of a smartphone. In both two modes, the pulsed carrier waveforms are modulated at the frequency of 10 Hz. Mode 2 is the high-dose treatment mode since it has longer pulse duration than the Mode 1 (Fig. 3b). The waveforms (zoom in Fig. 3b) demonstrate that the NFD has effectively transformed the initial NFC carrier waveform at 13.56 MHz (with the voltage oscillation range −10 V to 10 V) into the rectified carrier waveform at 27.12 MHz (same waveform required by the clinical PRFE treatment) at the voltage oscillation range between 5 V to 15 V. This result demonstrates that our PRFE-Bandage can generate the effective pulsed waveforms as required by the clinical PRFE treatment[19,57].

The electrical field strength of Mode 1 and Mode 2 are measured, where the radiation strength from the smartphone (Fig. 3c) and the receiving strength from the PRFE-Bandage (Fig. 3d) are illustrated. The results exhibit that there is a 50% attenuation of electromagnetic field strength from the transmission antenna on the smartphone to the reception antenna on the PRFE-Bandage at the targeted wound area (Fig. 3c: 2000 V/m vs. Fig. 3d: 1100 V/m). Nevertheless, within a working distance of 10 mm, the field strength (~300 V/m) measured from RER remains sufficient to conduct the wound healing (Fig. 3d) treatment[56]. Furthermore, Mode 2 consistently exhibits slightly higher average field strength as compared to Mode 1. This can be attributed to the prolonged pulse duration in Mode 2, which potentially enhances its therapeutic performance.

The PRFE radiation power density delivered at the wound site (with load resistor 100 ohm) for both PRFE-Bandages are illustrated in Supplementary Fig. 8 to Supplementary Fig. 10. Different rectifiers devices are tested and the KMB210F rectifier exhibits the best performance (power density = 162.4 mW/cm^2) and is selected to construct our NFD. The PRFE RER can generate enough electromagnetic energy for wound healing treatment (reported commercial PRFE therapy device ActiPatch with 73 mW/cm^2)[58]. The power density of PRFE-C Bandage was further measured under various load conditions, as illustrated in Fig. 3e and Supplementary Fig. 11. The results demonstrate that the PRFE-Bandage can still generate sufficient power density even when loading additional peripheral components, such as temperature sensors for wound monitoring. Not surprisingly, Mode 2 exhibits relatively higher power density with higher driving capabilities as compared to Mode 1, which leaves us enough margin and can be exploited for more sophisticated treatment varieties.

Durability tests under human daily wearing conditions

We characterized the mechanical performance of PRFE system under various human-wearing conditions, including folding, bending, wetting, heating and exposure to sweat. The bandage could recover to its original shape and exhibit < 16% of change in the electric field after 1000 cycles of folding (Fig. 3f). Additionally, the PRFE-Bandage performance remains stable when being bent from 0 to 180 degrees (< 8% variation, shown in Fig. 3g). This bending-invariance property is much more durable and flexible than those FPCB-based bandages[13,14] and PRFE treatment devices[21,47,52] previously reported. Even when the PRFE-Bandage is scrolled into a circle (bent to 360 degrees) (test images shown in Supplementary Fig. 12), the electric field strength in both modes can still reach to approximately 500 V/m (~60% variation, Fig. 3g), with still enough electric field strength for therapeutic treatments. The device also maintained a stable electric field strength after being immersed in water at three-hour intervals, reaching a continuous 24-h soak (< 15% variation) (Fig. 3h). Under sweat-imitating conditions using a 10 mM NaCl[59] solution at 37 °C, the device exhibited minimal field strength changes (< 12.3% after 1-h soaking, the treatment duration), though performance declined over extended exposure (variations of ~54.6% and ~43.0% for mode 1 and mode 2, respectively), as shown in Supplementary Fig. 13. Moreover, the RER-radiated electric field remained consistently stable as the bandage is heated from 25 °C to 90 °C during a water bath (Fig. 3i), showing the robustness under varying temperatures. Both PRFE-C and PRFE-L bandage (Supplementary Fig. 14 to Supplementary Fig. 17) demonstrate similar outcomes under these tests, Supplementary Table 4 and Supplementary Table 5 explicitly detail percentage variations of the electric field strength under each condition relative to the original state. Our PRFE-Bandage exhibits extraordinary flexibility and robustness under multiple wearing conditions and can endure the deformation caused by different body movements.

To evaluate the hydrogel's stability, weight loss was measured after one hour of exposure to various temperatures (4 °C, 25 °C, 37 °C, and 50 °C) (n = 3), simulating the daily treatment duration. Supplementary Fig. 18 reveals a linear increase in water loss rate with rising temperature. Importantly, at 37 °C (close to body temperature), the hydrogel exhibited a weight loss of less than 1.5%, demonstrating excellent stability during the treatment process.

Efficacy of cutaneous wound healing acceleration in SD rats

A series of preclinical animal experiments were conducted to assess the efficacy of our PRFE-Bandage in promoting the wound healing for various wound types. We first built two groups of rat models with circular (10 mm in diameter) or linear (10 mm in length) full-thickness skin wounds, respectively (Fig. 4a). To control for individual variation in wound healing capabilities among rats and ensure reliable experimental results, each rat model was given two back wounds (Supplementary Fig. 19): one treated with the appropriate PRFE-Bandage (PRFE-C for circular wound or PRFE-L for linear wound) and the other covered with a sterile, breathable, and electromagnetic-shielded dressing, serving as the control (see Fig. 4b and Supplementary Fig. 20a). A smartphone positioned 1 cm above the PRFE-Bandage. The PRFE treatment could be switched between two modes from the smartphone-APP to address the effects of different treatment doses on promoting wound healing (Supplementary Fig. 20b). For each group of modeling rats, half of them were treated with PRFE therapy one-hour every day under Mode 1 and the other half received Mode 2 treatment one-hour every day from the start. Figure 4c, d display the images of wound healing progression in the PRFE-C treatment group and PRFE-L treatment group under Mode 1 (orange boxes) and Mode 2 (green boxes). The images from the corresponding control group are also shown. Wound area reduction and relative wound size variation serve as important comparative metrics for evaluating the healing progress between control and treatment wounds[60]. Starting from Day 0 after the wound is formed, we can visually observe that for both circular and linear wounds, the treatment group exhibits faster healing process as compared to their respective control group, with smaller wound areas and drier wound surfaces during the complete healing process.

Figure 4e (left) displays the day-to-day relative wound sizes for both the PRFE treatment group and the control group. The wound size of the PRFE group shrinks more rapidly over the treatment period as compared to the control group, indicating a faster healing rate in the PRFE treatment group. The result suggests that PRFE-Bandage notably expedites the wound healing process, evidencing a marked therapeutic benefit. Figure 4e (middle) represents the disparity in wound closure rates between the PRFE-C treatment group and the corresponding control group for circular full-thickness skin wounds. Concurrently, Fig. 4e (right) represents the treatment efficacy of the PRFE-L Bandages for linear full-thickness skin wounds. It is noteworthy that all the results demonstrate their significant statistical power and marginal significance. Subsequent analysis of the areas under curve (AUC) further demonstrated that therapeutic effect of Mode 2 is superior to that of Mode 1, by achieving more acceleration in relative rates of wound closure (Mode 1 vs. Mode 2: 3.127 vs. 3.883 for circular wounds, and 2.921 vs. 3.302 for linear wounds, as displayed in Fig. 4f). This aligns with the initial hypothesis that the relatively higher power output of Mode 2 enhances its promoting effect on wound healing process.

Enhanced re-epithelialization and tissue regeneration

Temperature is a crucial factor throughout the wound healing process from early inflammation to late scar tissue remodeling, continuous temperature monitoring of the wounds was performed using an infrared thermometer, as depicted in Fig. 5a. Treatment wound (right) experienced slightly higher temperature on Day 3 because of earlier inflammation response. By Day 16, when complete healing was observed, its temperature aligned with that of the surrounding healthy tissue. Nonetheless, Fig. 5b illustrates that throughout the entire healing timeline, the anesthetic environment maintained consistent temperature profiles, resulting in no significant thermal differences between the treatment and control groups.

On the 16th day post-injury, tissue samples were collected from the central area of the wounds for detailed histological analysis. Hematoxylin and Eosin (H&E) staining at the wound site revealed that both the PRFE-treated and control wounds had undergone full epithelialization by the end of the experiment, showcasing continuous layers of epidermis and dermis observed in the wound region (Fig. 5c and Supplementary Fig. 21). This highlights the full-thickness dermal excision wound model allows for a comprehensive healing trajectory involving granulation tissue formation

and re-epithelialization, closely resembling the complex wound healing dynamics in human skin[60]. Notably, the PRFE-treated groups, both PRFE-C and PRFE-L, demonstrated enhanced epithelial regeneration and skin ductility at the wound center, as indicated by the considerably thicker epidermal layers compared to their respective controls (122 ± 4 μm vs. 75 ± 2 μm, $P < 0.001$, as illustrated in Fig. 5d, e). Additionally, the average width of the scar area in each PRFE-Bandage treated group was markedly reduced relative to their controls across diverse conditions (refer to Fig. 5f), signifying a tighter and more resilient union in the granulation tissue that underwent PRFE therapy.

Promotion in angiogenesis and cellular differentiation

On Day 16 after establishing the wound model, angiogenesis was quantitatively assessed using CD31 and α-SMA immunofluorescence staining. The concomitant expression of CD31 and α-smooth muscle actin (α-SMA) yielded insights into the vascular maturation at the wound site, reflecting both endothelial and smooth muscle cell development. Enhanced expression levels of CD31 and α-SMA were observed (Fig. 5g), indicating a significant rise in neovascularization and an increased microvessel density in the PRFE treated wounds. Figure 5h presents a quantitative comparison of CD31 and α-SMA levels between PRFE-treated and untreated tissue samples. The treated groups demonstrated a significant elevation in fluorescence intensity compared to the control ($P < 0.001$; Fig. 5h), corroborating the efficacy of PRFE therapy in promoting angiogenesis, as evidenced by the marked increment in microvessel formation in the treated wounds relative to the untreated wounds.

Discussion

The present study aims to address the limitations of conventional PRFE devices, which are often constrained by their large size, high costs, extended treatment durations, and frequent clinical visits—factors that collectively reduce efficacy and patient adherence. Through electromagnetic field measurements and animal studies, we demonstrate that our wearable, smartphone-enabled, and cost-effective PRFE-Bandage offers enhanced accessibility, affordability, and personalized treatment, achieving high therapeutic efficiency.

Compared to existing PRFE devices (Supplementary Table 2), our device excels in terms of the smaller size (footprint area: 13.5 cm² vs. 132.7 cm²)[47], lighter weight (0.34 g vs. 4535.9 g)[61], shorter and more cost-effective treatment duration (1 h/day vs. 2.5 h/day)[62], and lower manufacturing cost to their selling cost. One notable distinction lies in the device's portability and flexibility, which stand in sharp contrast to the rigid structures of traditional PRFE systems. Conventional PRFE devices often rely on stable power supplies or high-capacity batteries and feature sophisticated circuitry with solid-state components, factors that significantly lower treatment accessibility and patient compliance. Furthermore, our comparative analysis (Supplementary Table 6) highlights the superior performance of the PRFE system, offering superior electric field strength (1100 V/m vs. 530 V/m)[63] and enhanced cost-effectiveness ($1 vs. $18)[14] compared to most reported wireless wound healing systems. Inspired by advancements in materials, treatment modalities, and disease model innovations[63], our future work will focus on integrating these aspects to further enhance our system performance and adaptability.

The enhanced wound healing observed in the PRFE treatment group is attributed to the localized electromagnetic field generated by the bandage, which facilitates cellular migration, angiogenesis, and tissue regeneration. Our electromagnetic field measurements and animal studies confirmed its efficacy, demonstrating a significantly improved relative wound closure rates (4.2% vs. 21.5% at Day 12) and re-epithelialization (122 ± 4 μm vs. 75 ± 2 μm) after PRFE treatment compared to control groups. Additionally, Mode 2, characterized by longer pulse durations and higher power density, further amplified these therapeutic benefits, accelerating wound-healing process. In addition to its clinical efficacy, The PRFE-Bandage also exhibits mechanical stability, waterproofing, and thermal resistance, underscoring its potential as a user-centric and effective wound care solution. Notably, the
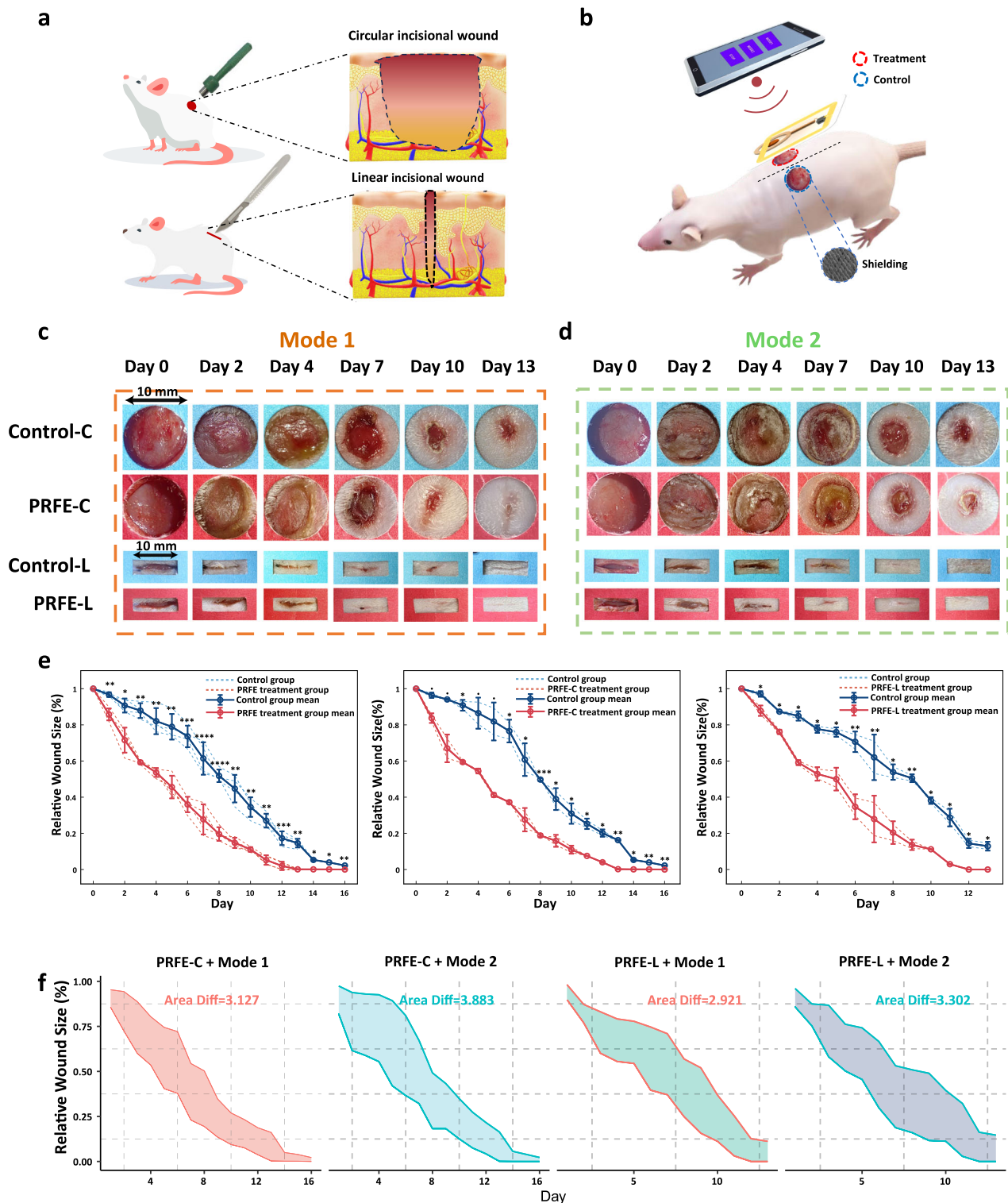
Fig. 4 | Therapeutic effects of PRFE in two treatment modes on full-thickness skin wounds in animal models. a Illustration for development of the full-thickness circular shaped skin wound (top) and linear incisional wound (bottom). **b** Schematic diagram of the test setup and PRFE treatment on a rat. **c** Wound healing process of PRFE-Bandage treatment group and the corresponding control group (top PRFE-C and bottom for PRFE-L) under treatment Mode 1. **d** Wound healing process of PRFE-Bandage treatment group and the corresponding control group (top PRFE-C and bottom for PRFE-L) under treatment Mode 2. **e** Relative wound size (with mean and variance) during the healing process for both circular and linear wounds (left), circular (middle) and linear (right) wounds under two modes. (For two-tailed paired *t*-test, **** indicates *P* < 0.0001, *** indicates *P* < 0.001, ** indicates *P* < 0.01, * indicates *P* < 0.05, and. indicates *P* < 0.1). **f** The average wound closure variations of all groups under two modes.
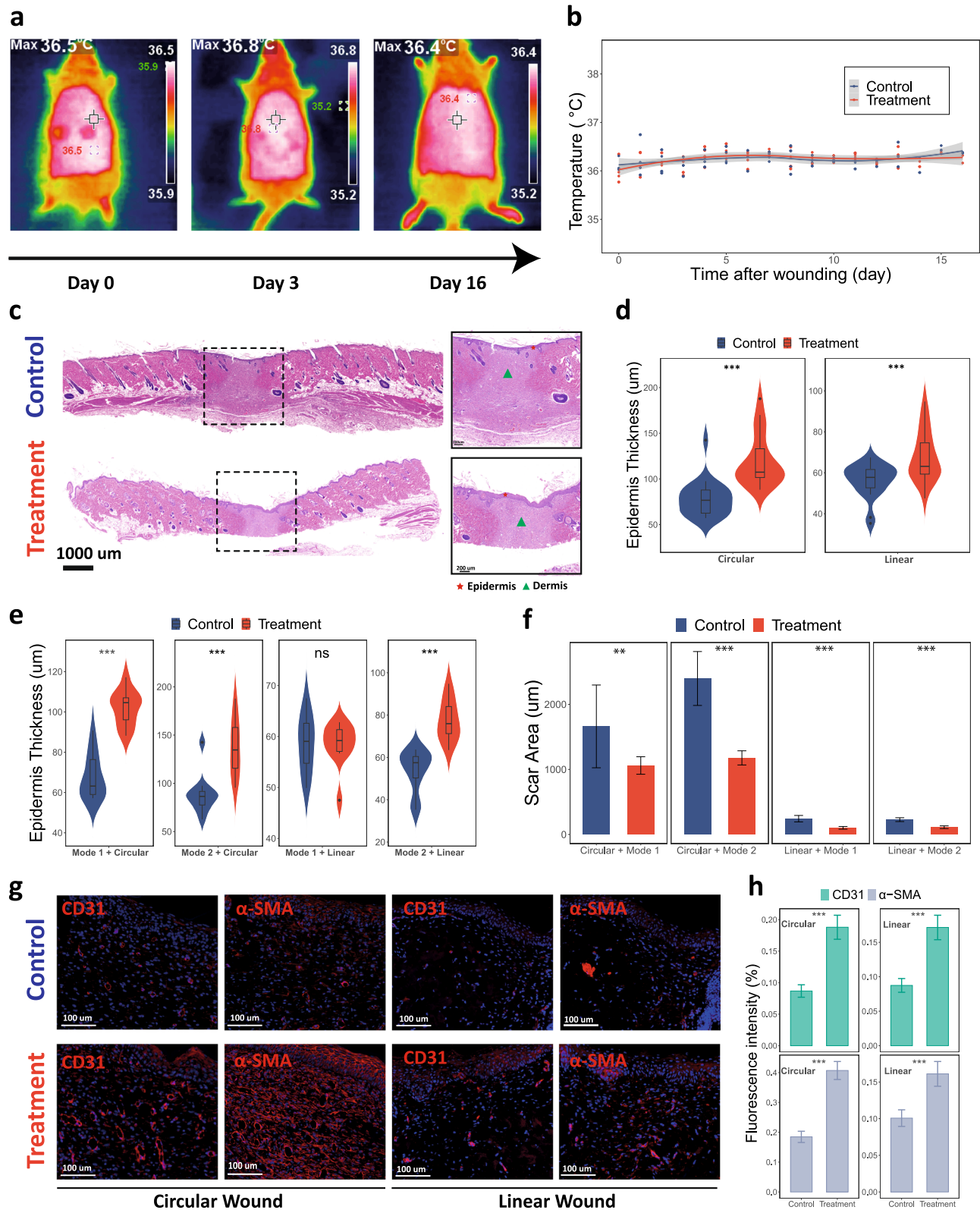
Fig. 5 | PRFE electrotherapy accelerates tissue regeneration and angiogenesis.
a IR images of the temperature distribution at different stages. **b** Daily average temperature of all treatment and control wounds. **c** Digital images of Histological (hematoxylin and eosin staining (H&E)) assessment of wound tissues on Day 16 after wounding. The black box highlights the wound area, showcasing the distribution of scar tissue and the status of the epidermis and dermis. **d** Quantification comparison of the epidermal thickness of all treatment and control wounds ($n = 10$).

e, **f** epidermal thickness (**e**) and scar area (**f**) for PRFE-C wound group, PRFE-L wound group, and the control wound group under two treatment modes.
g, **h** Immunostaining images (**g**) and quantitative comparison (**h**) of CD31 and α-SMA from the tissue of all treatment and control wounds. (For two-tailed paired t-test, **** indicates $P < 0.0001$, *** indicates $P < 0.001$, ** indicates $P < 0.01$, * indicates $P < 0.05$, indicates $P < 0.1$, and ns indicates $P > 0.1$ (no significance)).

PRFE device may also prove effective in treating complex wounds, such as diabetic ulcers[13]; however, this requires rigorous validation through well-designed future studies.

This study has also identified areas in need of further optimization. First, the polyimide protective layer used in the device offers limited breathability, necessitating ongoing efforts to explore alternatives such as fabric-based substrates to enhance user comfort. Second, while the one-hour continuous treatment protocol demonstrated consistent therapeutic delivery under controlled conditions, its practicality for everyday human use requires refinement. Potential approaches include designing a fabric cushion to support smartphones without interfering with NFC radiation or creating wearable smartphone holders for hands-free operation. Additionally, segmented treatment schedules could be explored to enhance convenience without sacrificing efficacy. Third, although our results suggest that Mode 2's higher power density and longer pulse duration enhance therapeutic outcomes, the specific dose-response relationship remains to be quantified and warrants further investigation to optimize treatment parameters.

Overall, the development of a smartphone-enabled PRFE-Bandage presents a low-cost, smartphone administered alternative to traditional PRFE systems. The device's personalized and flexible design ensures adaptability to a wide range of wound conditions, effectively bridging the gap between clinical efficacy and patient convenience. Electromagnetic field simulations and measurements confirmed that the proposed PRFE-bandage achieves the strength of clinical-grade PRFE equipment. Additionally, the animal experiments validated its effectiveness in promoting wound healing, re-epithelialization and angiogenesis. Future clinical studies will also be essential for evaluating the economic viability, durability, and the potential for further miniaturization of its electronic components in the real-world context.

Methods

Design and fabrication of a wireless and cost-effective PRFE-Bandage

The custom-designed flexible PRFE Bandage is engineered on a dual-layer, flexible copper-clad PI substrate, employing the ISO 9001-certified FPCB manufacturing process. An ultra-thin, surface-mounted SOP-4 bridge rectifier (model KMB210F) is affixed to one side of the substrate via tin-lead solder paste, followed by hot air reflow soldering for robust attachment. A six-turn NFC antenna coil is strategically positioned atop the substrate to facilitate communication coupling with smartphones. Concurrently, the configuration and dimensions of the radiation electrode, customized to align with the wound model's specifications, are designed on the underside of the FPCB. The entire device is encapsulated in a biocompatible and skin-friendly material (adhesive hydrogel), (JieRui, II), ensuring safe direct contact with the wound surface. The weight loss rate of hydrogel was measured after one hour of exposure to different temperatures in a temperature-controlled incubator to evaluate its stability to temperature variations. The prototype dimensions are established at 51.3 mm × 26.3 mm. To achieve waterproof integrity, UV-curable adhesive is applied to the soldering points, and the assembly is subjected to a 10-min curing process under a commercial UV lamp. The finalized PRFE system has full reusability, with a BOM (only one Bridge Rectifier) and manufacturing cost approximating US$0.75 and encapsulating hydrogel material cost of US$0.21 per unit, culminating in a total cost of roughly US$0.96 per PRFE-Bandage. Supplementary Table 7 includes an itemized list of all electrical components, materials, and the overall manufacturing cost of FPCB fabrication and assembly per device.

The electromagnetic characterization of antenna coils was analyzed using the commercial software CST Studio Suite 3D EM simulation and analysis software. The device maintains stable communication up to 30 mm, ensuring efficient energy transfer for wound therapy with optimal privacy at a distance of 10 mm. Electromagnetic parameters of copper from the CST material library were utilized, applying adaptive mesh convergence with polyhedral mesh elements for enhanced accuracy. Characterization of the

NFC coil was conducted via dual-port scattering analysis to derive the equivalent scattering parameters. Subsequently, the input impedance (Z_{in}) was calculated as a function of frequency, facilitating the extraction of the quality factor (Q) through the following formula[64–66]:

$$Z_{in} = Z_0 \frac{1 + S_{11}}{1 - S_{11}} \tag{1}$$

$$Q = \frac{\Im[Z_{in}]}{\Re[Z_{in}]} \tag{2}$$

where $Z_0 = 50\ \Omega$ represents the characteristic impedance of the vector network analyzer and transmission cables. The resonate frequency and the Q-factor of PRFE-Bandage were measured using an HF/LF Tag Tester (QBG5C, AI). The Tester is a specialized instrument for evaluating the performance of NFC antennas. A signal generator generates a sinusoid Continuous Wave (CW) with the frequency sweeping from 3 MHz to 30 MHz. The CW signal is fed into a transceiver antenna that couples with the PRFE-bandage. The strength of the coupled signal from PRFE-bandage is measured at every step of the frequency sweeping. In order to eliminate the reflection of CW wave from the transceiver antenna, the reflection signal strength is also measured without the presence of the PRFE bandage. The reflection signal strength is used to calibrate the coupling signal from the PRFE bandage therefore the real coupling signal can be extracted. The frequency response of the coupled signal strength from the PRFE bandage sweeping from 3 MHz to 30 MHz can be measured through this tester and the Q-factor can be derived as:

$$Q = \frac{f_r}{\Delta f} \tag{3}$$

where f_r is the resonant frequency (the peak value of the response), and Δf is the bandwidth between the −3 dB points on the frequency response curve.

Smartphone-programable treatment setting

The two distinct treatment modes are preprogrammed and switchable through our developed Android APP. This APP was designed on Android Studio mainly by calling the NFC adapter class, NFC package and some functions in Android to regulate the duty cycle for enabling and disabling NFC signal transmission. These modes essentially utilize square amplitude modulation on the carrier wave to produce pulsed envelope waves at a frequency of 10 Hz. Prior study[12] had demonstrated the therapeutic efficacy of wound healing and pain alleviation using PRFE at low frequency ranging from 1 Hz–30 Hz. In this study, the averaged pulse frequency at 10 Hz is used. Mode 1 is defined by a 30 ms NFC signal 'on' period followed by a 70 ms 'off' period for each pulse cycle, whereas Mode 2 extends the 'on' period to 60 ms with a reduced 'off' period of 40 ms. The therapeutic doses of PRFE are determined by the duty cycle parameter, i.e., the on-off ratio of the pulses. Without loss of generality, Modes with two duty cycles, i.e., low duty cycle of 30% (Mode 1) and high duty cycle of 60% (Mode 2), had been implemented, which correspond to relatively low field strength and high field strength.

FEA and calculation for characterization of RER

The FEA for assessing the electric field distribution induced by the RER within a cutaneous wound scenario was conducted using the commercial software COMSOL 5.2a (COMSOL Multiphysics® software, COMSOL Inc.). To achieve computational accuracy, we employed a strategy incorporating a triangular mesh for convergence analysis, coupled with a box radiation boundary. This approach facilitated the analysis of potential distribution and electric field modules for elucidating the electromagnetic characteristics when subjected to rectified AC signals at a frequency of 27.12 MHz. The constructed model of a cutaneous wound encompassed a wound domain measuring 10 mm in diameter and 1.1 mm in thickness, accompanied by successive layers representing the epidermis (0.1 mm

thick), dermis (1 mm thick), adipose tissue (1 mm thick), and muscle (3 mm thick). The simulation domain was characterized by a fluid stimulating the dielectric properties of blood, alongside detailed thickness and material specifications for skin layers[67].

The FEA applied to the Bio-heat equations and the Electric field equations[67–69], combined with existing computational software, can be utilized to solve for the current density vector field $\boldsymbol{j}$, electric potential $\boldsymbol{\Phi}$, electric field $\boldsymbol{E}$, and the distribution of bio-heat surrounding RER on the skin. The computation of the electric field $\boldsymbol{E}$ surrounding RER is governed by Maxwell's equations[11]:

$$\mathbf{j} = \sigma\mathbf{E} \tag{4}$$

$$\nabla \cdot \left(\sigma + i\omega\varepsilon\varepsilon_0\right)\mathbf{E} = 0 \tag{5}$$

$$\mathbf{E} = Ee^{i\omega t}\mathbf{u} \tag{6}$$

Here, σ is the specific electrical conductivity of the tissue, $i = \sqrt{-1}$, $\omega = 2\pi f$, $\varepsilon_0 = 8.85 \times 10^{-12} F/m$ and ε represents the relative permittivity of the skin tissue. $\boldsymbol{u}$ is the unit vector of $\boldsymbol{E}$. Integrating Gauss's Law and the charge conservation, currents induced by time-varying magnetic fields are not considered. The specific calculations and parameters used in the calculations are detailed in the Supplementary Information and Supplementary Table 3.

Mechanical performance and durability testing

The mechanical durability of the PRFE system was tested under conditions imitating human wear, including folding, bending, wetting, and heating. The PRFE bandage underwent mechanical deformation (e.g., bending at angles between 0° and 360° (different bending radii using 3D-printed molds) and environmental exposure, such as immersion in water or saline solution and heating in a water bath. To ensure measurement accuracy, all performance evaluations were conducted in a radio-frequency anechoic chamber to eliminate external electromagnetic interference. The device was powered wirelessly using a smartphone, and the electric field strength was measured at a distance of 10 mm above the electrodes using the high-frequency electromagnetic radiation meter (DELIXI, DLY-1701), a portable instrument capable of precise field intensity measurements ($n = 10$). All tests were performed without the hydrogel encapsulation on the bandage to assess its intrinsic mechanical resilience.

Bending tests employed molds fabricated using polylactic acid (PLA), a biodegradable polymer, designed to match the bandage's dimensions (parameters in Supplementary Table 8). During water immersion tests at 25 °C, the electric field strength was measured every three hours up to 24 h, confirming stable performance after prolonged soaking. For robustness under sweat conditions, a 10 mM NaCl solution (imitating human sweat) prepared with 0.05 mol/L NaCl was used, and measurements were conducted in a 37 °C incubator. All experiments were repeated multiple times, and the average electric field strength was recorded. The results confirmed that the PRFE bandage maintained consistent performance under mechanical and environmental stresses, supporting its suitability for wearable applications.

The sterile, adhesive hydrogel (JieRui, II) used for secure attachment during treatment, its weight loss rate was measured after one hour of exposure to different temperatures (4 °C, 25 °C, 37 °C, and 50 °C) in a temperature-controlled incubator. Hydrogel samples ($n = 3$) matching the PRFE-Bandage's area were unsealed and placed in sealed petri dishes before incubation, and the weight loss rate was calculated as the percentage difference between the initial and final weights.

$$R = \frac{\left(W_0 - W_t\right)}{W_0} \tag{7}$$

where W_0 is the initial weight of the hydrogel sample after unsealing, and W_t is the weight of the hydrogel after 1 h at a specific temperature.

Animal diets and full-thickness wound modeling

All Female Sprague-Dawley (SD) rats (aged six weeks) were individually housed under consistent environmental conditions within a temperature-regulated facility at 22 °C, subject to a 12-h light/dark cycle, and provided libitum access to water and standard rodent diet. These animals were subjected to identical wound surgeries and housed under identical management practices. The conduct of all animal-related experimental protocols received prior approval from the Southern University of Science and Technology (SUSTech) Animal Ethics Committee. These studies were executed within the confines of the SUSTech Animal Center Laboratory, in strict accordance with the institution's guidelines, to ensure the welfare and humane care of the animals throughout the experimental duration.

All Sprague-Dawley rats were anesthetized using a 2% to 3% isoflurane induction, followed by maintenance on 1.5% to 2% isoflurane. Prior to the surgical creation of wounds, each rat received a subcutaneous injection of the analgesic carprofen at a dosage of 4 mg kg^{-1}. Preparing for the procedure, rats were placed in a ventral position, and the hair on their dorsal surfaces was removed using electric clippers before being further depilated to ensure uniformity. The skin was then disinfected with an alcohol solution after a five-minute interval. To mitigate the impact of intrinsic healing variability among the subjects and ensure dependable results, each rat model was given two dorsal wounds: one designated for treatment with the specialized PRFE-Bandage (PRFE-C for circular wounds, PRFE-L for linear wounds) and the other covered with a sterile, electromagnetic shielding dressing for control purposes. During animal experiments, adhesive sterile gauze (Cofoe, Wuhan) was used to secure the PRFE device, addressing adhesion challenges due to the rats' fur. The PRFE-treatment was consistently applied to the right-sided wounds, while the left-sided wounds were used as controls. The positioning of dorsal wounds was strategically chosen to avoid self-inflicted damage by the rats, reducing the probability of secondary complications. After each treatment session, both treatment and control wounds were covered with sterile gauze to shield them from environmental exposure and potential infection during the period of individually housed.

PRFE treatment and recording at wound sites

Randomly assigning SD rats with circular wound models into PRFE-C Mode 1 treatment group and PRFE-C Mode 2 treatment group ($n = 4$). Similarly, rats with linear wound models were randomly assigned into PRFE-L Mode 1 treatment group and PRFE-L Mode 2 treatment group ($n = 4$). Under 2% isoflurane inhalation anesthesia, the right wounds of all rats covered the corresponding PRFE-Bandage and received 1-h PRFE treatment administered by a smartphone (OPPO Reno 1) each day, while the left wounds covered with electromagnetic shielding material (as control) received no additional treatment. To achieve the maximum power transfer efficiency, we securely fixed the smartphone on a 3D-printed adjustable stand, positioned precisely 10 mm directly above the device. This setup ensured consistent signal strength and minimized variability.

The progression of wound status was continuously monitored over the healing period. Temperature monitoring at both the treated and control wound sites was performed using an infrared thermometer, the PRFE treatment and mode switching were conducted using the smartphone APP. Photographic of wounds were captured with the digital camera on a smartphone (OPPO Reno 1). Wound area measurements were initiated immediately following wound model establishment (Day 0) and were subsequently conducted daily from Day 1 through Day 16. For the quantification of daily wound area changes (WA_x), Image J software (National Institutes of Health, USA) was employed. The calculation of the relative wound area percentage ($RW\%$) was based on the following formula:

$$\text{RW}(\%) = \frac{WA_x}{WA_0} \times 100\% \tag{8}$$

Histological and immunofluorescence staining

Euthanasia was administered to the SD rats upon the healing of their treatment-induced wounds. For the PRFE-L group, this procedure was conducted on Day 14, while for the PRFE-C group, it took place on Day 16, employing an overdose of ketamine and xylazine for the purpose. Subsequently, wound tissues were excised from the regenerated areas (both the treated and control regions) located on the same dorsal surface of the rats using a biopsy punch (10 mm in diameter), in a manner similar to the technique employed in the creation of a full-thickness wound model.

Specimens underwent fixation in paraformaldehyde phosphate-buffered saline before paraffin embedding. Subsequently, sections of approximately 5 μm thickness were prepared and subjected to routine H&E staining, facilitating the examination of epithelialization, cellular composition, and granulation tissue alterations at the wound interface. Additionally, the fixation of frozen skin samples was carried out in cold acetone, followed by washes in cold PBS. Immunohistochemical techniques were applied to formalin-fixed, paraffin-embedded skin samples, with specific stains for CD31 and α-SMA to gauge their expression levels. The thickness of granulation and epithelial tissues was quantitatively assessed at ten systematically distributed points surrounding the wound center for each specimen, utilizing Case Viewer software for measurement. Additionally, ImageJ software facilitated the quantitative evaluation of CD31 and α-SMA expression, offering insights into neovascularization and inflammatory response alterations.

Statistical analysis

Categorical data were summarized as frequencies and percentages; continuous data were summarized as means and standard deviation (SD). To evaluate the statistical significance and power of experiments, two-tailed paired t-tests were conducted on experimental data pertaining to relative wound size variations and pathological studies. Significance levels were denoted as follows: '****' for $P < 0.0001$, '***' for $P < 0.001$, '**' for $P < 0.01$, '*' for $P < 0.05$, and '·' for $P < 0.1$.

Data availability

All data used in this work are present in the main section of the paper or the Supplementary Information. Data are also available from the corresponding authors upon request.

References

1. Martin, P. Wound healing–aiming for perfect skin regeneration. *Science* **276**, 75–81 (1997).
2. Singer, A. J. & Clark, R. A. Cutaneous wound healing. *N. Engl. J. Med.* **341**, 738–746 (1999).
3. Frykberg, R. G. & Banks, J. Challenges in the treatment of chronic wounds. *Adv. Wound Care* **4**, 560–582 (2015).
4. Tribble, D. R. et al. After the battlefield: infectious complications among wounded warriors in the Trauma Infectious Disease Outcomes Study. *Mil. Med.* **184**, 18–25 (2019).
5. Chen, C. et al. Photothermal-promoted multi-functional dual network polysaccharide hydrogel adhesive for infected and susceptible wound healing. *Carbohydr. Polym.* **273**, 118557 (2021).
6. Chen, H. et al. Dissolved oxygen from microalgae-gel patch promotes chronic wound healing in diabetes. *Sci. Adv.* **6**, eaba4311 (2020).
7. Werdin, F., Tenenhaus, M. & Rennekampff, H.-O. Chronic wound care. *Lancet* **372**, 1860–1862 (2008).
8. Zhao, M. et al. Electrical signals control wound healing through phosphatidylinositol-3-OH kinase-γ and PTEN. *Nature* **442**, 457–460 (2006).
9. Park, D.-W. et al. Electrical neural stimulation and simultaneous in vivo monitoring with transparent graphene electrode arrays implanted in GCaMP6f mice. *ACS Nano* **12**, 148–157 (2018).
10. Yu, M. et al. e-Bandage: exploiting smartphone as a therapeutic device for cutaneous wound treatment. *Adv. Intell. Syst.* **6**, 2300494 (2024).
11. Cosman Jr, E. R. & Cosman Sr, E. R. Electric and thermal field effects in tissue around radiofrequency electrodes. *Pain Med.* **6**, 405–424 (2005).
12. Guo, L., Kubat, N. J. & Isenberg, R. A. Pulsed radio frequency energy (PRFE) use in human medical applications. *Electromagn. Biol. Med.* **30**, 21–45 (2011).
13. Song, J. W. et al. Bioresorbable, wireless, and battery-free system for electrotherapy and impedance sensing at wound sites. *Sci. Adv.* **9**, eade4687 (2023).
14. Jiang, Y. et al. Wireless, closed-loop, smart bandage with integrated sensors and stimulators for advanced wound care and accelerated healing. *Nat. Biotechnol.* **41**, 652–662 (2023).
15. Reid, B. & Zhao, M. The electrical response to injury: molecular mechanisms and wound healing. *Adv. Wound Care* **3**, 184–201 (2014).
16. Yu, R., Zhang, H. & Guo, B. Conductive biomaterials as bioactive wound dressing for wound healing and skin tissue engineering. *Nano-Micro Lett.* **14**, 1–46 (2022).
17. Hunckler, J. & De Mel, A. A current affair: electrotherapy in wound healing. *J. Multidiscip. Healthc.* **20**, 179–194 (2017).
18. Pang, Q. et al. Smart flexible electronics-integrated wound dressing for real-time monitoring and on-demand treatment of infected wounds. *Adv. Sci.* **7**, 1902673 (2020).
19. Fu, T., Lineaweaver, W. C., Zhang, F. & Zhang, J. Role of shortwave and microwave diathermy in peripheral neuropathy. *J. Int. Med. Res.* **47**, 3569–3579 (2019).
20. Ilfeld, B. M., Said, E. T., Abdullah, B. & Finneran Iv, J. J. Treating intractable postamputation pain with noninvasive, wearable, nonthermal, pulsed shortwave (radiofrequency) therapy: a 12-patient case series. *Am. J. Case Rep.* **23**, e937549–937541 (2022).
21. Rawe, I. M. & Vlahovic, T. C. The use of a portable, wearable form of pulsed radio frequency electromagnetic energy device for the healing of recalcitrant ulcers: a case report. *Int. Wound J.* **9**, 253–258 (2012).
22. Mostafalu, P. et al. A textile dressing for temporal and dosage controlled drug delivery. *Adv. Funct. Mater.* **27**, 1702399 (2017).
23. Long, Y. et al. Effective wound healing enabled by discrete alternative electric fields from wearable nanogenerators. *ACS Nano* **12**, 12533–12540 (2018).
24. Bogie, K. M. The modular adaptive electrotherapy delivery system (MAEDS): an electroceutical approach for effective treatment of wound infection and promotion of healing. *Mil. Med.* **184**, 92–96 (2019).
25. Yao, G. et al. A programmable and skin temperature–activated electromechanical synergistic dressing for effective wound healing. *Sci. Adv.* **8**, eabl8379 (2022).
26. Baniya, P. et al. A system for bioelectronic delivery of treatment directed toward wound healing. *Sci. Rep.* **13**, 14766 (2023).
27. Qin, X. et al. Triboelectric-responsive drug delivery hydrogel for accelerating infected wound healing. *Adv. Healthcare Mater.* **13**, 2303474 (2024).
28. Xu, G. et al. Battery-free and wireless smart wound dressing for wound infection monitoring and electrically controlled on-demand drug delivery. *Adv. Funct. Mater.* **31**, 2100852 (2021).
29. De Loecker, W., Cheng, N. & Delport, P. Effects of pulsed electromagnetic fields on membrane transport in Emerging Electromagnetic Medicine (eds. O'Connor, M.E., Bentall, R.H.C., Monahan, J.C.) 45–57 (Springer, 1990).

30. Ross, J. Biological effects of pulsed high peak power electromagnetic energy using diapulse in Emerging Electromagnetic Medicine (eds. O'Connor, M.E., Bentall, R.H.C., Monahan, J.C.) 269 (Springer, 1990).

31. Song, B. et al. Application of direct current electric fields to cells and tissues in vitro and modulation of wound electric field in vivo. *Nat. Protoc.* **2**, 1479–1489 (2007).

32. Kao, H.-K. et al. Collagen synthesis modulated in wounds treated by pulsed radiofrequency energy. *Plast. Reconstr. Surg.* **131**, 490e–498e (2013).

33. Asci, H. et al. Combined pulsed magnetic field and radiofrequency electromagnetic field enhances MMP-9, Collagen-4, VEGF synthesis to improve wound healing via Hif-1α/eNOS pathway. *Aesthetic Plast. Surg.* **47**, 2841–2852 (2023).

34. Martino, M. M. et al. Growth factors engineered for super-affinity to the extracellular matrix enhance tissue healing. *Science* **343**, 885–888 (2014).

35. Ruiz-Fernández, A. R. et al. Nanosecond pulsed electric field (nsPEF): opening the biotechnological Pandora's box. *Int. J. Mol. Sci.* **23**, 6158 (2022).

36. Vieira, A. C. et al. Ionic components of electric current at rat corneal wounds. *PLoS One* **6**, e17411 (2011).

37. Kubat, N. J., Moffett, J. & Fray, L. M. Effect of pulsed electromagnetic field treatment on programmed resolution of inflammation pathway markers in human cells in culture. *J. Inflamm. Res.* **8**, 59–69 (2015).

38. Phillips, J. L. Effects of electromagnetic field exposure on gene transcription. *J. Cell. Biochem.* **51**, 381–386 (1993).

39. Jordan, S. et al. Pulsed radiofrequency in interventional pain management: cellular and molecular mechanisms of action–an update and review. *Pain Physician* **24**, 525 (2021).

40. Choi, H. M., Cheing, A. K., Ng, G. Y. & Cheing, G. L. Effects of pulsed electromagnetic field (PEMF) on the tensile biomechanical properties of diabetic wounds at different phases of healing. *PLoS ONE* **13**, e0191074 (2018).

41. Goudarzi, I., Hajizadeh, S., Salmani, M. E. & Abrari, K. Pulsed electromagnetic fields accelerate wound healing in the skin of diabetic rats. *Bioelectromagnetics* **31**, 318–323 (2010).

42. Abd Elrashid, N. A., Hamada, H. A., Abdelmoety, A. M., Soliman, G. & Abbas, R. Additional effect of pulsed electromagnetic fields to laser therapy on management of diabetic foot ulcer: a single blind randomized controlled trial. *Biosci. Res.* **15**, 3322–3328 (2018).

43. Porreca, E. G. & Giordano-Jablon, G. M. Treatment of severe (Stage III and IV) chronic pressure ulcers using pulsed radio frequency energy in a quadriplegic patient. *Eplasty* **8**, e49 (2008).

44. Li, Q. et al. Pulsed radiofrequency energy accelerates wound healing in diabetic mice. *Plast. Reconstr. Surg.* **127**, 2255–2262 (2011).

45. Ginsberg, A. Pulsed short wave in the treatment of bursitis with calcification. *Int. Rec. Med.* **174**, 71–75 (1961).

46. Al-Mandeel, M. M. & Watson, T. Pulsed and continuous shortwave therapy in Electrotherapy: evidence-based practice, Edn. 12th (ed. Waston, T.) 137–178 (Elsevier, 2008).

47. Ilfeld, B. M. et al. Wearable, noninvasive, pulsed shortwave (radiofrequency) therapy for analgesia and opioid sparing following outpatient surgery: a proof-of-concept case series. *Pain Practice* **23**, 553–558 (2023).

48. Bianchi, N. et al. Use of pulsed radiofrequency electromagnetic field (PRFE) therapy for pain management and wound healing in total knee and reverse shoulder prosthesis: randomized and double-blind study. *EuroMediterranean Biomed. J.* **13**, 120–126 (2018).

49. Frenkel, V. & Li, K. C. Potential role of pulsed-high intensity focused ultrasound in gene therapy. *Future Oncol.* **2**, 111–119 (2006).

50. Ojango, C., Raguso, M., Fiori, R. & Masala, S. Pulse-dose radiofrequency treatment in pain management—initial experience. *Skeletal Radiol.* **47**, 609–618 (2018).

51. Tabakan, I., Yuvacı, A. U., Taştekin, B., Öcal, I. & Pelit, A. The healing effect of pulsed magnetic field on burn wounds. *Burns* **48**, 649–653 (2022).

52. Rawe, I. M., Lowenstein, A., Barcelo, C. R. & Genecov, D. G. Control of postoperative pain with a wearable continuously operating pulsed radiofrequency energy device: a preliminary study. *Aesthetic Plast. Surg.* **36**, 458–463 (2012).

53. Han, G. & Ceilley, R. Chronic wound healing: a review of current management and treatments. *Adv. Ther.* **34**, 599–610 (2017).

54. Luigi, C. & Tiziano, P. Mechanisms of action and effects of pulsed electromagnetic fields (PEMF) in medicine. *J. Med. Res. Surg.* **1**, 1–4 (2020).

55. Kalidasan, V. et al. Wirelessly operated bioelectronic sutures for the monitoring of deep surgical wounds. *Nat. Biomed. Eng.* **5**, 1217–1227 (2021).

56. Saw, T. B. et al. Transepithelial potential difference governs epithelial homeostasis by electromechanics. *Nat. Phys.* **18**, 1122–1128 (2022).

57. Lv, H. et al. Magnetic fields as a potential therapy for diabetic wounds based on animal experiments and clinical trials. *Cell Proliferation* **54**, e12982 (2021).

58. Brook, J., Dauphinee, D. M., Korpinen, J. & Rawe, I. M. Pulsed radiofrequency electromagnetic field therapy: a potential novel treatment of plantar fasciitis. *J. Foot Ankle Surg.* **51**, 312–316 (2012).

59. Choi, D.-H., Kim, J. S., Cutting, G. R. & Searson, P. C. Wearable potentiometric chloride sweat sensor: the critical role of the salt bridge. *Anal. Chem.* **88**, 12241–12247 (2016).

60. Galiano, R. D. et al. Quantitative and reproducible murine model of excisional wound healing. *Wound Repair Regen.* **12**, 485–492 (2004).

61. Sorrell, R. G., Muhlenfeld, J., Moffett, J., Stevens, G. & Kesten, S. Evaluation of pulsed electromagnetic field therapy for the treatment of chronic postoperative pain following lumbar surgery: a pilot, double-blind, randomized, sham-controlled clinical trial. *J. Pain Res.* **11**, 1209–1222 (2018).

62. Markov, M. S. Expanding use of pulsed electromagnetic field therapies. *Electromagn. Biol. Med.* **26**, 257–274 (2007).

63. Kaveti, R. et al. Water-powered, electronics-free dressings that electrically stimulate wounds for rapid wound closure. *Sci. Adv.* **10**, eado7538 (2024).

64. Cho, S. et al. Wireless, battery-free, optoelectronic diagnostic sensor integrated colorimetric dressing for advanced wound care. *Adv. Funct. Mater.* **34**, 2316196 (2024).

65. Finkenzeller, K. RFID handbook: fundamentals and applications in contactless smart cards, radio frequency identification and near-field communication. (John Wiley & Sons, 2010).

66. Seo, D. W., Lee, J. H. & Lee, H. S. Study on two-coil and four-coil wireless power transfer systems using Z-parameter approach. *ETRI J.* **38**, 568–578 (2016).

67. Johnson, C. R. Numerical Methods for Bioelectric Field Problems in The Biomedical Engineering Handbook, Edn. 2nd (ed. Bronzino, J. D.) 162–180 (CRC, 1995).

68. Singh, S. & Melnik, R. in Computational Science–ICCS 2019: 19th International Conference, Faro, Portugal, June 12–14, 2019, Proceedings, Part IV 19 436–450 (Springer, 2019).

69. Fan, J. & Wang, L. A general bioheat model at macroscale. *Int. J. Heat Mass Transf.* **54**, 722–726 (2011).

Acknowledgements

Author contributions

M.Y., H.J.Y., and H.T.Y. contributed equally to this work. T.T.Y. conceived and supervised this project. M.Y. and H.J.Y. performed circuit design and testing. M.Y. and H.T.Y. conducted simulation. M.Y., S.L., H.T.Y., H.D. and

Competing interests

The authors declare no competing interests.

Additional information

Supplementary information The online version contains supplementary material available at https://doi.org/10.1038/s41746-025-01462-z.

Correspondence and requests for materials should be addressed to Yongxin Guo, John S. Ho or Terry Tao Ye.

Reprints and permissions information is available at http://www.nature.com/reprints

Publisher's note Springer Nature remains neutral with regard to jurisdictional claims in published maps and institutional affiliations.